THE JOURNAL OF PHYSICAL CHEMISTRY C

Article

pubs.acs.org/JPCC

Fabrication of Highly Stable, Hybrid PbS Nanocomposites in PAMAM Dendrimer Matrix for Photodetection

Srabanti Ghosh, Ali Hossain Khan, and Somobrata Acharya*

Centre for Advanced Materials, Indian Association for the Cultivation of Science, Jadavpur, Kolkata 700032, India

Supporting Information

ABSTRACT: A novel dendrimer-templating one step method for the in situ synthesis of hybrid nanocomposites of lead sulfide (PbS) quantum dots (QDs) of average diameter of 2.5−4.5 nm in poly(amidoamine) dendrimer matrix (PAMAM) at ambient condition is reported here. The PbS QDs are developed in cubic crystallographic phase with a high degree of crystallinity. FTIR analysis confirm a direct evidence of PbS QDs linkage to the surface functional groups of dendrimer molecules, which provides a way to prevent the aggregation tendency of the PbS QDs retaining the original properties in 3D rigid dendrimer matrix. Additionally, the thermal stability of dendrimer molecule increases in the nanocomposite unit indicating strong interaction of inorganic phases with dendrimer. The as-prepared PbS nanocomposites could be stored for three months at 4 °C retaining original optical characteristics. The synthesis route provides a simplified colloidal route for producing monodisperse hybrid PbS nanocomposites with robust optical properties. Pure dendrimer is photo inactive, while upon white light irradiation, the PbS nanocomposites results in enhanced photocurrent compared to the dark measurement. Repetitive on−off device response upon white light illumination is found to be sharp and repeatable over successive on/off irradiation cycles. The photoresponse of PbS nanocomposites promises application in photoswitching and photosensitive detectors.

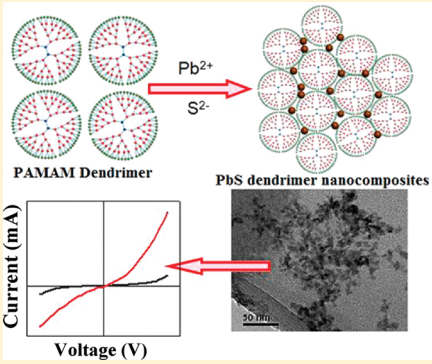

1. INTRODUCTION

The combination of inorganic and organic or bioactive components with nanomaterial has created an immense new area in materials science prospecting extraordinary implications in the development of multifunctional materials.[1] The concept of hybrid organic−inorganic material has been exploded recently, where a mild synthesis route allows the design of a variety of hybrid materials.[2] Dendrimer is a unique macromolecule with highly branched backbones and a large number of internal or external functional groups, which provide an opportunity to fabricate monodispersed nanomaterials with controlled morphologies.[3] Multifunctional dendrimers endow unique potential in the synthesis of hybrid organic−inorganic materials and may serve concomitantly as nanoreactors, stabilizers, and site-specific templates.[3,4] The amalgamation of biocompatibility and nonimmunogenity of dendrimer with semiconductor QDs could yield novel hybrid materials ideally suitable for a broad range of applications such as catalysis, sensors, nanoelectronics, and biomedical devices.[5,6] Furthermore, versatile solubility of the nanocomposite in various solvents promises robust applications in electronic, optical spectroscopy, and catalysis. The uses of dendrimer as a capping agent also improves the chemiccal performance of the nanoparticle surface via protection against oxidation and reduced toxicity specifically for cadmium- and lead-based nanomaterials.

Along the line of concept, a variety of type II−VI semiconductor QDs have been reported using dendrimer matrix.[7,8] However, reports on the preparations of type IV−VI lead chalcogenides QDs using a dendrimer matrix is limited, and the photoresponse of such novel nanocomposite materials is relatively unexplored.[9] Lead sulfide (PbS) is one of the most important low band gap semiconductors possessing unique chemical, physical, and optoelectronic properties useful in infrared detectors, optical fiber, infrared lasers ,and solar energy harvesting.[10,11] Easy processability in both the aqueous and organic medium and tailorable functionality of the dendrimer molecule make this organic−inorganic hybrid concept more interesting. Several effective strategies were deployed to prepare lead sulfide QDs in different environments such as zeolites, porous glass, micelles, membranes, polymers, or in colloidal state.[12−14] The high quality PbS QDs are typically prepared at elevated temperature with organic capping agents such as oleic acid, trioctylamine, trioctylphosphine oxide, hexadecylamine, etc., through organometallic synthesis. For example, monodispersed shape controlled PbS QDs were recently successfully synthesized via thermolysis of single source precursor by our group.[15] However, the organic stabilizers are detrimental for device fabrication purposes. Additionally, functionalization of the capping agent is required to bind the nanomaterials to a substrate;[16] otherwise, chemically reactive substrate is essential.[17] In contrast, dendrimer-mediated synthesis exhibits a

Received: November 11, 2011
Revised: February 22, 2012
Published: February 24, 2012

greater degree of control with respect to their composition, size, shape, and surface functionalities, which in turn, imparts stability and prevents agglomeration. In this regard, the numerous reactive groups on the surface of dendrimers can be used to render the composites soluble in essentially any solvent and easily can be immobilized by adsorption or by printing on a variety of substrates enabling control on self-assembly.[6] Interestingly dendrimer can fulfill the criteria of capping agent providing a plethora for controllable nanotools along with the ability to target desired chemical, physical, or biological environments.[18] To date, dendrimer mediated synthesis of PbS QDs was first reported by Ime et al.; however, no definite parameters were outlined for controlling the particle characteristics.[9] Complete understanding of the nanohybrid structures from different perspectives still remains a great challenge. Nanometer scale PbS QDs in the dendrimer matrix may be useful for fabricating novel sensors and microelectronic devices.

In the present study, we have endeavored to synthesize highly crystalline, stable, functionalized PbS/dendrimer nanocomposites. PbS QDs with average diameter of 2.5 to 4.5 nm are designed in cubic crystallographic phase with a high degree of cystallinity. The resultant nanocomposite displays optical properties corresponding to PbS QDs. The variation of dendrimer concentration, generation, and terminal groups can effectively control the stability and optical properties of PbS QDs formed in the dendrimer matrix. FTIR analysis reveals that PbS QDs are bound to the surface functional groups of dendrimer molecules in contrast to earlier reports where the semiconductor nanocrystals are formed randomly in the interior or at the periphery. Thermal stability of the dendrimer molecule increases in the nanocomposite unit indicating strong interaction of inorganic phases with dendrimer. In order to measure photoresponse, a hybrid PbS/dendrimer nanocomposite-based device has been successfully fabricated. Photocurrent response of these devices upon white light irradiation was measured. The current increases sharply upon illumination of light resulting in orders of enhanced current compared to the dark measurements. The device constructed using the nanocomposites show high photoswitching performance and is promising for large-area photodetector applications. In addition, these photoactive nanocomposites are important for biocompatible optoelectronic devices considering high cellular uptake and target specificity of the dendrimer molecule.[19,20]

2. EXPERIMENTAL SECTION

Starburst polyamidoamine (PAMAM) dendrimer of different generations (G2.0, G4.0, and G5.0) having surface hydroxyl groups, G4.0 with trimethoxysilyl end groups, G4.0 with amino end groups, and lead nitrate were purchased from Sigma Aldrich, USA, and sodium sulfide (Na_2S) were obtained from Merck, India. Indium tin oxide (ITO) substrates (70−100 Ω/squares inches) were purchased from Aldrich. All chemicals used were of analytical grade or of high purity available. Milli-Q water (Millipore) and methanol (HPLC grade) were used as solvents. On the basis of the manufacturer's value of the dendrimer weight fractions in methanol and the known dendrimer densities, we prepared a dendrimer stock solution of 2.0×10^{-4} M in methanol.

2.1. Synthesis of PbS/Dendrimer Nanocomposites. A typical preparation of PbS/dendrimer nanocomposites with an initial Pb^{2+}/S^{2-} molar ratio of 1:0.5 was as follows: 5 mL aliquot of Pb^{2+} stock solution was added to 10 mL of dendrimer stock solution at 25 °C and vigorously stirred for 30 min. Then, a freshly prepared aqueous solution of Na_2S (1.0×10^{-3} M) was added in stoichiometric amount to the N_2 purged solution mixture of Pb^{2+} and dendrimer. The reaction mixture was stirred vigorously during this addition and for 30 min after the addition. The solutions were stored at 4 °C and were stable for several weeks without any precipitate, change in color, or changes in their optical properties.

The effect of supersaturation on the quality of dendrimer nanocomposites was studied by preparing different sets (5 mL each) of Pb−dendrimer solution with concentrations of Pb^{2+} ions as 2.0×10^{-3} M and 6.0×10^{-3} M in which the molar ratio of dendrimer:Pb^{2+}:S^{2-} was, however, kept constant. It caused the initial supersaturation to increase, although the number of ligands available for each monomer remained the same. The degree of supersaturation corresponding to the 2.0×10^{-3} M Pb^{2+} ions has been denoted as S, which is used for relative scaling of supersaturation.

Thin film was fabricated on a top of ITO coated glass simply by spin-casting using an as-prepared PbS nanocomposite solution. Sandwiched pattern devices were fabricated by depositing aluminum by a vacuum deposition technique as the back electrode.

Transmission electron microscopy (TEM), high-resolution TEM (HRTEM), selected area electron diffraction (SAED), powder X-ray diffraction (XRD), ultraviolet (UV)−visible(vis) absorption spectra, photoluminescence spectrophotometer, dynamic light scattering spectrophotometer (DLS), Fourier transformation infrared spectroscopy (FTIR), and thermo gravimetric analyzer (TGA) were used to characterize the size, binding, structure, and thermal stability of synthesized PbS nanocomposites. UV−vis absorption spectra were recorded on a Shimadzu UV-1601PC spectrophotometer. An absorption spectrum of dendrimer stabilized PbS QDs was obtained taking the absorption of pure dendrimer as blank. Transmission electron microscopy was carried out on JEOL JEM-2010 with an acceleration voltage of 200 kV. A drop of as-prepared solution PbS QDs was placed on a carbon-coated copper grid and dried before putting it on to the TEM sample chamber. XRD measurements of QDs were performed by a Rigaku XRD instrument (λ = 1.5405 Å). A square wave pulse of 100 Hz was applied during RT measurement, and the voltage of the pulse was varied from 0 V to 10 V. Scanning rate of 0.02° per seconds in 2θ range from 20−60° were employed. The FTIR spectra were recorded with Perkin-Elmer Spectrum GX equipment with a resolution of 2 cm^{-1} and scan range of 1000−4000 cm^{-1}. Size distribution and zeta potential of PbS/dendrimer nanocomposites was determined by DLS spectrophotometer (Model DLS-nanoZS, Zetasizer, Nanoseries, Malvern Instruments). The zeta potential was calculated from the electrophoretic mobility using the Smoluchowski equation with the help of commercial software. The results are expressed as mean values of three samples. Zeta potential measurements were performed at 25 °C. TGA measurement was performed by a TGA 2850 thermo gravimetric analyzer (TA Instruments) under N_2 in the temperature range of 30−800 °C with an increasing rate of 5 °C/min. For photocurrent response measurements, the current flowing through the device was estimated by measuring a voltage drop (measured using Agilent Model No. 34970A) across 56 kΩ sensing resistance. The light source for photocurrent response measurement was a 200 W tungsten lamp, and the light intensity was measured by a

dx.doi.org/10.1021/jp210856n | J. Phys. Chem. C 2012, 116, 6022−6030

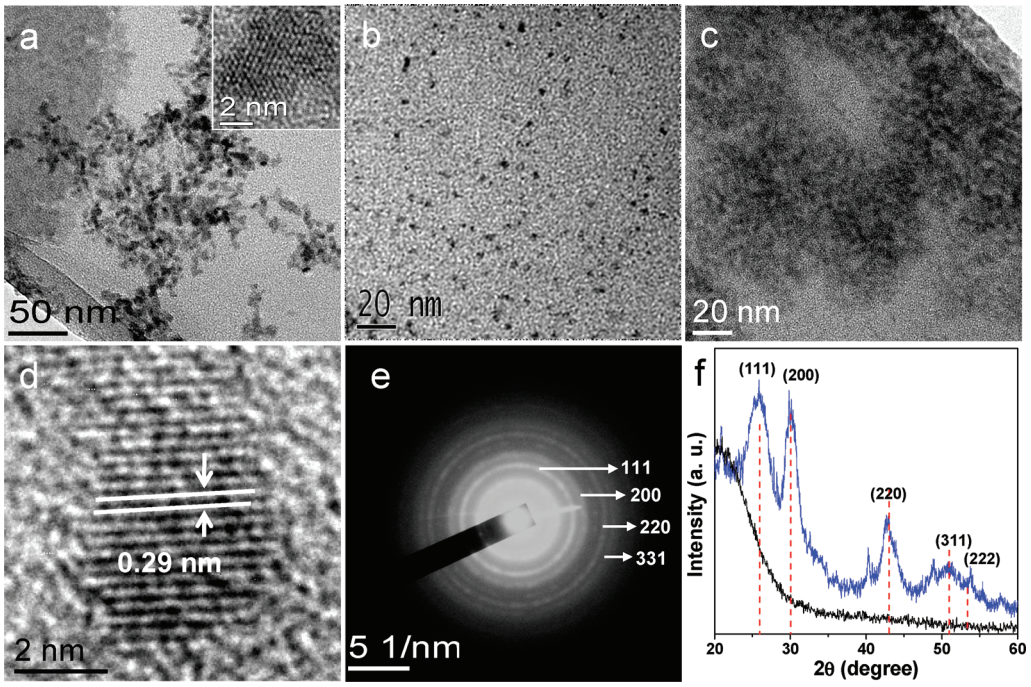

Figure 1. TEM image of PbS/dendrimer nanocomposites (PbS/G4.NH_2) at two different supersaturation (1S and 3S) using NH_2-terminated dendrimers, (a) PbS/G4.NH_2 at 1S and (b) PbS/G4.NH_2 at 3S. Inset of panel a: HRTEM image of the corresponding PbS QDs. (c) The TEM images of nanocomposites using OH-terminated dendrimer at 3S. (d) HRTEM image of PbS QDs in the dendrimer matrix using OH-terminated dendrimer at 3S. The lattice spacings are marked with the lines and arrows. (e) The SAED pattern of PbS QDs using OH-terminated dendrimer. The corresponding planes are indexed within the figure. (f) The XRD patterns of the OH-terminated dendrimer (black curve) and corresponding PbS/dendrimer nanocomposites (blue curve). The positions and intensities of the standard peaks of rock-salt cubic PbS (JCPDS #05-0592) are indicated by vertical red dotted lines.

calibrated lux meter (Kyoritsu Electrical Instruments Work Ltd. Tokyo, model 5200).

3. RESULTS AND DISCUSSION

We have used two different types of dendrimers, namely, OH-terminated and NH_2 dendrimers for the synthesis of PbS nanocomposites. Figure 1a,b shows TEM images of PbS QDs using the NH_2-terminated dendrimer at two different supersaturations (1S and 3S) (details are described in the experimental section).[21] The supersaturation of initial reaction mixture was varied by changing the absolute concentration of each of the reagents, while keeping the molar ratio of reagents fixed at 1:20:10 for dendrimer:Pb^{2+}:S^{2-}. Notably, the size distribution of the QDs focused with a 3-fold increase in initial supersaturation as evident from the TEM image (Figure 1a,b). We interpret this result in terms of the simple correlation between critical particle size and supersaturation (eq 1).[22]

At a given time of growth, there exists a critical radius with zero growth rate, which remains in equilibrium with respect to particle growth. Such radius can be defined as

$$r_{cr} = \frac{2\gamma V_m}{RT \ln S} \quad (1)$$

where r_{cr} is the critical radius, γ the specific surface energy of the particles, V_m the molar volume of solid, and supersaturation $S = [M]_{bulk}/C^{\circ}_{flat}$, where $[M]_{bulk}$ is the concentration of PbS monomers in the bulk of solution and C°_{flat} is the solubility of the bulk material. The r_{cr} would be the smallest for a nanoparticle solution with the highest degree of supersaturation. If the critical size is smaller than the size of the smallest particle present in the ensemble, all particles will show positive growth rate, and smaller crystals within the ensemble grow faster than the larger ones leading to focusing of size distribution.[23]

At higher supersaturation, due to availability of a larger number of nucleation centers and controlled growth of the PbS QDs in the dendrimer matrix, agglomeration is prevented within the reaction system as evident from Figure1b. The average size of PbS QDs at 1S supersaturation is found to be ~4.5 nm, while at 3S supersaturation, particles are slightly smaller (~4.0 nm) as estimated from TEM images. The crystallinity of the material is evident from the high-resolution TEM image (inset of Figure 1a), showing well resolved lattice fringes. An energy dispersive X-ray spectroscopy elemental analysis spectrum (EDS) reveals a stoichiometric ratio of Pb to S (see Figure S-1, Supporting Information).

A typical TEM image for PbS/dendrimer nanocomposites using OH-terminated dendrimer is shown in Figure1c. The size of the PbS QDs (~2.5 nm) synthesized using OH-terminated dendrimer is smaller in comparison to PbS QDs using NH_2-terminated dendrimer (Figure 1a,b). At lower supersaturation (1S), PbS QDs results in aggregated structure upon using OH-terminated dendrimer (Figure S-2, Supporting Information). PbS QDs in the OH-terminated dendrimer at different supersaturation follow the same trend as PbS QDs in NH_2-terminated dendrimer; however, PbS QDs in NH_2 dendrimer matrix show better dispersity. This may be due to differential electrostatic interaction between Pb and terminal groups of the dendrimer molecules in the precursor complexes, which further influences the overall growth and dispersity of PbS QDs. Figure 1d shows the HRTEM image of PbS QDs in the OH-terminated dendrimer matrix. Prominent lattice planes

dx.doi.org/10.1021/jp210856n | J. Phys. Chem. C 2012, 116, 6022–6030

appeared indicating that the PbS QDs are highly crystalline in nature. The spacing between adjacent lattice planes is found to be 0.29 nm, which can be indexed to (200) planes of cubic PbS structure (JCPDS # 5-0592) (Figure 1d). The selected area electron diffraction (SAED) pattern supports cubic phase with (200), (220), and (311) diffraction planes (Figure 1e). These structural results show that the PbS QDs synthesized using dendrimer matrix is in cubic crystallographic phase with growth direction along the ⟨200⟩ axis.

The crystallographic phase of the PbS QDs is further verified using XRD. A comparison of XRD patterns of the pure OH-terminated dendrimer and PbS nanocomposites using OH-terminated dendrimer is shown in Figure 1f. A control experiment with pure dendrimer lacks an effective peak in the XRD pattern. The XRD of PbS nanocomposites using OH-terminated dendrimer shows a high degree of crystallinity with predominant (111), (200), and (220) reflections. Most of the peaks match well with Bragg reflection conditions of the standard face-centered cubic (fcc) structure of bulk PbS (JCPDS #05-0592). The intense (200) diffraction peak indicates that the nanocomposites are abundant in {100} facets and grow along the ⟨200⟩ directions. These results of XRD analysis are well consistent with HRTEM and SAED diffraction pattern.

FTIR was implied to study the chemical affinity of PAMAM dendrimer toward the surface of the PbS QDs. PAMAM dendrimers are highly branched organic polymers that have different reaction sites at the interior and periphery. Dendrimer is composed of core, repetitive unit [−N−(CH_2−CH_2−CONH−CH_2−CH_2)$_2$−] and terminal groups, which provide different functionalities to the QDs. The structural components of dendrimer with different terminal groups are shown in Figure 2. Figure 2a,b shows PAMAM dendrimers with NH_2 and

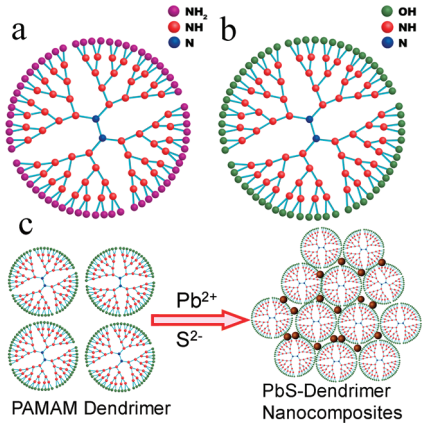

Figure 2. Schematic representation of PAMAM dendrimer structure with (a) amine (NH_2) and (b) hydroxyl (OH) terminal groups. The blue, red, purple, and green balls represent core amine (N), secondary amine of repetitive unit (NH), terminal NH_2, and terminal OH groups of dendrimer, respectively. (c) Synthesis scheme of PbS QDs in the OH-terminated dendrimer matrix, where brown balls represent the PbS QDs.

OH terminal groups, respectively, and the formation scheme of PbS QDs within the dendrimer matrix is shown in Figure 2c.

Figure 3 shows that the FTIR spectra of PAMAM dendrimer with −NH_2 and −OH groups and PbS nanocomposites using these dendrimers, respectively. The spectra of both −NH_2- and −OH-terminated pure PAMAM dendrimer shows a broad band in the range of 3300−3400 cm^{-1} corresponding to −NH stretching vibrations. The peaks in the range of 1560 cm^{-1} and 1637 cm^{-1} can be readily assigned to the amide I and amide II (the coupling between bending of N−H and stretching of C−N bands, respectively). The peaks related to −CH_2 and −CH_3 groups of dendrimer appear in the range of 2800−3000 cm^{-1}. The FTIR spectrum for OH-terminated dendrimer also shows peaks in the same range of NH_2-terminated dendrimer (Figure 3c,d); however, a marginal shift has been observed. Note that the amide I (1637 cm^{-1}) and amide II (1560 cm^{-1}) peaks of pure NH_2-terminated dendrimer remain nearly identical for PbS QDs synthesized using NH_2-terminated dendrimer. However, the band at 3286 cm^{-1} in NH_2-terminated dendrimer is shifted to 3364 cm^{-1} for PbS QDs synthesized using NH_2-terminated dendrimer. This particular band can be assigned to the stretching mode of the surface amine group (NH_2) of the dendrimer, and the observed shift can be assigned due to the coordination of NH_2 to the Pb atoms.

According to the relative location of nanoparticles within or on the surface of dendrimers, three different types of nanocomposites may exist; (i) nanoparticles inside dendrimers (internal type); (ii) nanoparticles at the surface of the dendrimers (external type); and (iii) random distribution at the surface and inside the dendrimer (mixed type).[3,4] The nature of the nanocomposite depends on the interactions between the metal ions and by the reaction pathways for the formation of the nanoparticles. Thus, dendrimers can be utilized either as nanoreactors (templates with internal cavities, i.e., internal type) or as stabilizers (external type). Furthermore, the band at 3280 cm^{-1} in OH-terminated dendrimer can be attributed to the stretching mode of the surface hydroxyl group shifted to 3318 cm^{-1} for PbS QDs synthesized using OH-terminated dendrimer. This suggests the coordination of OH to the Pb atoms. Our FTIR results implies that the PbS QDs are attached to the surface NH_2 and OH groups of the dendrimer structure forming external type composites for both types of dendrimers. Note that our results are in shear contrast with the previously studied semiconductor nanoparticles such as CdS, CdTe, and ZnTe where a more pronounced interaction with the C−N bond manifested through a significant shift in both the amide I and amide II vibrations forming a mixed type composite.[24,25] In our case, the dendrimer can be used as a ligand for nanoparticle stabilization owing to the presence of surface coordinating groups.

The formation of the external type of nanocomposites is further corroborated with dynamic light scattering (DLS) measurements. Figure 4a illustrates the size distribution histogram of PbS nanocomposites using OH-terminated dendrimer. The histogram reveals a size distribution ranging from 7.8 to 11.5 nm. Note that the DLS measurements are sensitive to the entire size of the nanocomposite including the dendrimers.

Recall that TEM images reveal an average size of 2.5 nm for the PbS QDs within the nanocomposite. The experimentally obtained hydrodynamic diameter of G4.0 PAMAM dendrimer is calculated to be ∼4.5 nm in methanol. We can estimate a cross-sectional width of ∼11.5 nm of a single nanocomposite from a simple model (Figure 4a, inset) considering the diameter of the dendrimers at the periphery of 2.5 nm PbS QDs. The geometric model is in close match with the nanocomposite size estimated from the DLS measurements. The model also implies that the inter PbS interactions is minimized in such configuration, a feature advantageous in

dx.doi.org/10.1021/jp210856n | J. Phys. Chem. C 2012, 116, 6022−6030

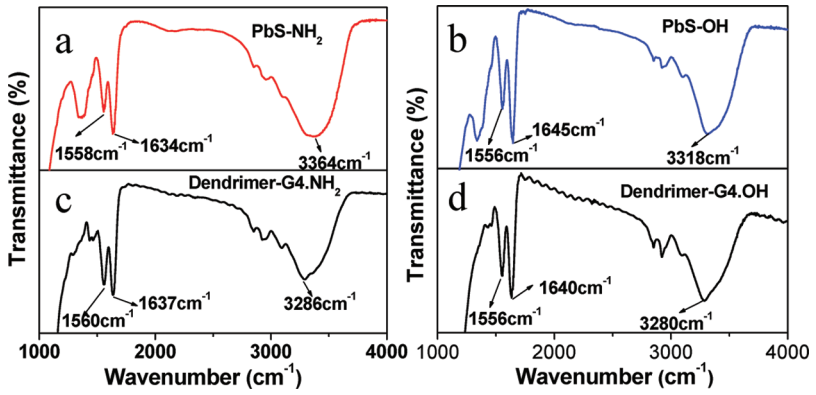

Figure 3. FTIR spectra of PbS/dendrimer nanocomposites produced by using (a) NH_2-terminated dendrimer (red curve) and (b) OH-terminated dendrimer (blue curve). FTIR spectra of pure dendrimer with (c) NH_2 terminal groups (black curve) and (d) OH terminal groups (black curve).

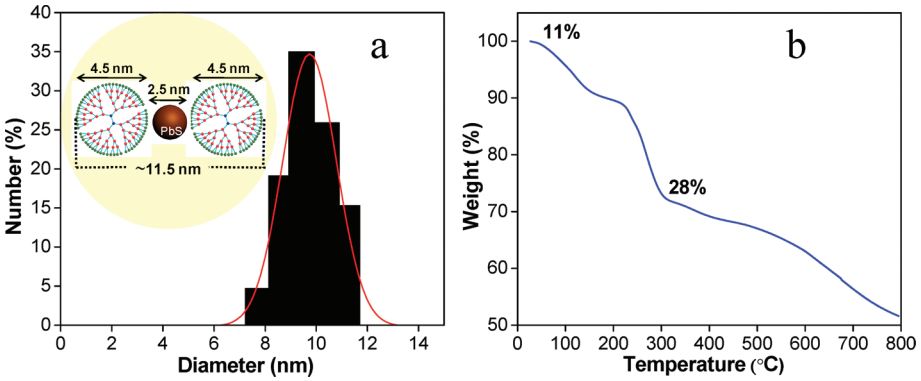

Figure 4. (a) Size distribution histogram of PbS/dendrimer nanocomposites with OH-terminated dendrimer by dynamic light scattering. Inset: schematic representation of cross-sectional width of a single nanocomposite. (b) TGA profile of PbS/dendrimer nanocomposites using OH-terminated dendrimer.

producing monodisperse nanocomposites. In contrast to previous reports, where aggregation of nanocomposites were frequently observed,[26,9] our PbS/dendrimer nanocomposite shows better dispersity owing to the external type nature and steric hindrance between the neighboring dendrimer molecules. The synthesized PbS nanocomposites are exceptionally stable for months of storage in dark as verified from DLS measurements.

TGA was carried out on PbS nanocomposites to testify the stability with temperature (Figure 4b). The TGA graph shows 11% weight loss up to 100 °C. A second transition is observed at 215 °C, and a weight loss of approximately 28% up to 300 °C is observed, while the weight loss is 38% up to 600 °C. Dendrimer molecules are thermosensitive, and it has been reported that at 550 °C, PAMAM dendrimers are fully decomposed through retro-Michael reaction in the presence of oxygen and metals.[27] In the present case, the end-product is quite stable as indicated by the plateau in the thermogram. The actual concentrations of PbS units in nanocomposites is calculated to be 34% taking into account the dendrimer molecular weight of 14 277 (~66%) in the net composite sample. While the decomposition of PbS starts around 440 °C,[28] 28% of the dendrimer fraction remains in the composites up to 600 °C. Similar results were obtained in the case of other polymer−semiconductor nanocomposites,[29] where the thermal stability is improved up to 100 °C. In our composite, formation of PbS QDs significantly affects the stability of dendrimer matrix, which results in residual mass of dendrimer even at 600 °C.

PbS/dendrimer nanocomposites show an emission peak at 560 nm upon excitation at 400 nm (Figure 5), which accounts for the formation of PbS QDs. In order to evaluate the effect of dendrimer concentrations on the photoluminescence (PL) intensity of nanocomposite, sets of experiments were carried out where the concentrations of the dendrimer capping agent and the inorganic ions were varied in steps.

First, the concentration of Pb^{2+} and S^{2-} ions were kept fixed at 2×10^{-3} M and 1×10^{-3} M, respectively, and the concentration of PAMAM dendrimer was varied from 5×10^{-5} M to 4×10^{-4} M for effective passivation of PbS QDs. The PL intensity increases with dendrimer concentration initially for the $[Pb^{2+}]$ to [dendrimer] ratio of ~1:0.025 to 1:0.075 (Figure 5) reaching a saturation, and then it gradually decreases upon further increase of the dendrimer concentration (from 1:0.15 to 1:0.2). These control experiments suggest that PAMAM dendrimer of 2×10^{-4} M is required for optimum PL intensity. The observed enhancement of PL intensity with this dendrimer concentration further implies that 2×10^{-4} M dendrimer passivates PbS QDs surfaces efficiently and imparts stability to the PbS/dendrimer nanocomposites. Interestingly, PL intensity of nanocomposites is significantly increased upon aging compared to a freshly prepared PbS composite (Figure S-3, Supporting Information). Such enhancement of the PL intensity is possibly owing to better surface passivation with time.

Figure 6a shows absorption spectra of PbS/dendrimer nanocomposites using different sulfide ratio ($[Pb^{2+}]:[S^{2-}] \approx$ 1:0.25 to 2) for fixed lead (2×10^{-3} M) ions and dedrimer ($2 \times$

dx.doi.org/10.1021/jp210856n | J. Phys. Chem. C 2012, 116, 6022−6030

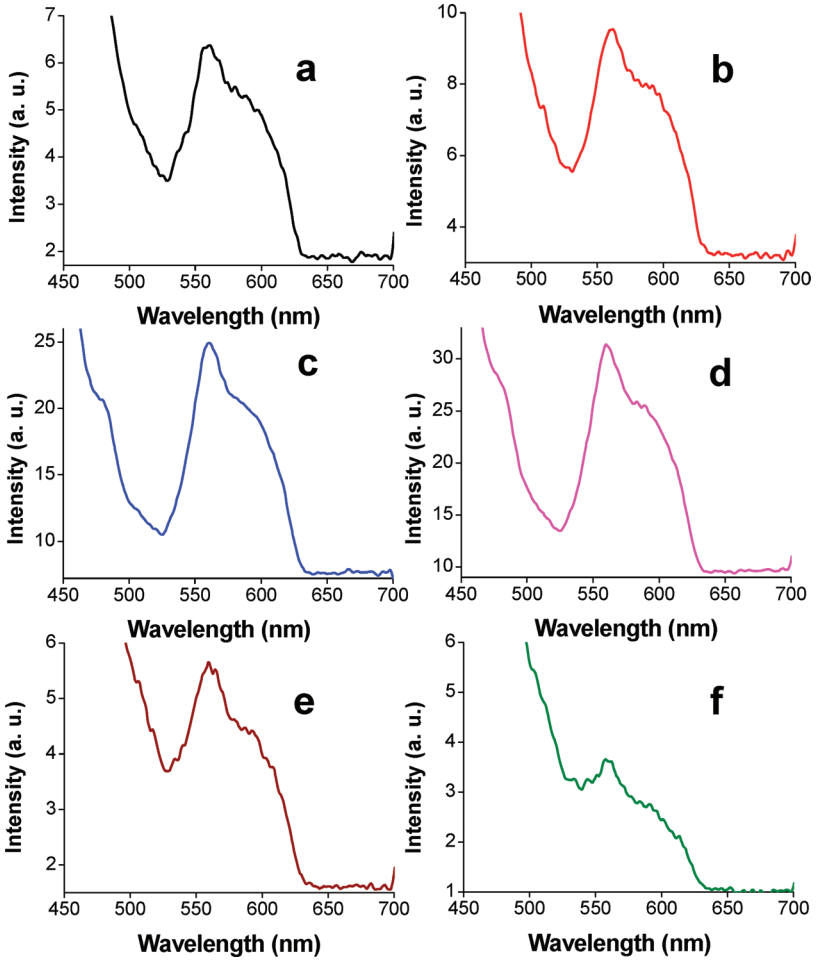

Figure 5. Photoluminescence spectra of PbS/dendrimer nanocomposites with varying concentration of dendrimer. The concentration of Pb^{2+} ions was fixed at 2×10^{-3} M and the Pb^{2+} to dendrimer ratio was maintained at (a)1:0.025, (b) 1:0.05, (c) 1:0.075, (d) 1:0.1, (e) 1:0.15, and (f) 1:0.2, respectively. For comparison, the PL intensities are presented in original scale.

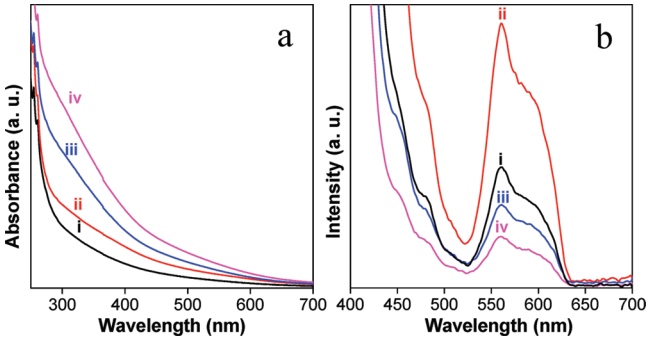

Figure 6. (a) UV−vis absorption and (b) PL spectra of PbS/dendrimer nanocomposites (using OH-terminated dendrimer) with varying Pb^{2+} to S^{2-} molar ratio of (i) 1:0.25, (ii) 1:0.5, (iii) 1:0.75, and (iv) 1:1, respectively.

10^{-4} M). Absorption spectrum shows a broad absorption feature indicating that the change in molar ratios did not affect the particle size or distribution. The absorption feature of the PbS/dendrimer nanocomposite is overall shifted toward lower wavelengths compared to the bulk PbS. However, further increase in the molar ratio ($[Pb^{2+}]:[S^{2-}] \approx 1:2$) results in precipitation of the as-prepared PbS QDs in the dendrimer martix within few minutes. It is worth noticing that concentration of sulfide ion affects the PL intensity significantly (Figure 6b).

The PL intensity increases up to 1×10^{-3} M of sulfide concentration and then quenches upon further increase in the sulfide molar ratio. At higher concentration of sulfides ($[Pb^{2+}]:[S^{2-}] \approx 1:1$), the excess S^{2-} ions competes with the OH groups of the dendrimers, which tend to bind to the Pb^{2+} ions. However, the coordination of dendrimer hydroxyl with the cationic sites on PbS QDs is weaker compared to the Pb^{2+} to S^{2-} interaction. The excess of S^{2-} ions creates intermediate states through which radiative transition takes place thereby reducing the PL intensity (Figure 6b).

In order to examine the influence of dendrimer surface groups on the nanocomposite formation, we have used PAMAM dendrimer functionalized with different terminal groups such as amino ($-NH_2$), hydroxyl ($-OH$), and trimethoxysilyl [$Si(OCH_3)_4$]. Out of these three terminal groups, $Si(OCH_3)_4$ is easily hydrolyzable and used as nanoscale scaffolds for building sol−gel materials.[30,31] Three different nanocomposites were prepared under identical synthesis conditions at 25 °C for a fixed molar ratio of $[Pb^{2+}]:[S^{2-}] \approx 1:0.5$. The emission intensity of PbS nanocomposites is affected by the terminal group of the dendrimer (Figure S-4, Supporting Information). The bright PL corresponding to PbS QDs are obtained with OH- or NH_2-terminated dendrimers due to stronger coordinating ability to Pb^{2+} in comparison to the

dx.doi.org/10.1021/jp210856n | J. Phys. Chem. C 2012, 116, 6022−6030

$Si(OCH_3)_4$ group. Strong electrostatic interaction between Pb^{2+} and NH_2 or OH groups also controls the growth and stabilization of the PbS QDs more efficiently than $Si(OCH_3)_4$-terminated dendrimer molecules, which certainly provides the opportunity to modulate further functionalities for practical applications of functional nanocomposites.

We also investigated the effect of the dendrimer generation on the stability of the nanocomposites. PbS/dendrimer nanocomposites were prepared using three different generations (G2.0, G4.0, and G5.0) of the NH_2-terminated dendrimer. The nanocomposites prepared using different dendrimer generations display enhanced PL intensity for higher generations (Figure S-5, Supporting Information). A significant difference was observed in the stability of the nanocomposites synthesized using a different generation of dendrimers. The solutions containing nanocomposites of G2.0 PAMAM dendrimer formed a precipitate within one week at 4 °C. The nanocomposites with the G4.0 dendrimer were stable for approximately six weeks at 4 °C, while the G5.0 dendrimer is the most stable (up to twelve weeks), indicating that larger dendrimers provided better stability to the nanocomposites owing to the different number of functional groups and structural differences. It is interesting to note that the dendrimer of lower generation tends to exist in relatively open forms, which is detrimental in controlling PbS QD growth. Higher generation dendrimers take a spherical three-dimensional structure that appreciably controls nucleation and growth of the PbS QDs.

The stability of nanocomposites can be measured by estimating the surface charges using the zeta potential. A higher surface charge or high value of zeta potential means that he nanoparticles are electrostatically repulsive to one another, and thus, nanoparticles are more stable in solution.[32] The surface charge of the as prepared PbS/dendrimer nanocomposites was measured by the electrophoretic mobility, which depends on the terminal groups of the dendrimer (Table 1).

Table 1. Zeta Potential of PbS/Dendrimer Nanocomposites with Amino ($-NH_2$), Hydroxyl ($-OH$), and Trimethoxysilyl [$Si(OCH_3)_4$] Terminal Groups and with Different Pb^{+2} to S^{-2} Ratios

materials	zeta potential (mV)
PbS-G4.OH (Pb^{2+}:S^{2-})	
1:0.25	29.0
1:0.5	37.0
1:0.75	43.0
1:1	21.0
1:2	12.0
PbS-G4.NH_2	34.0
PbS-G5.NH_2	45.0
PbS-G4.Si[O−CH_3]$_4$	24.0

Primary NH_2-terminated PbS nanocomposites using G4.0 dendrimer are positively charged (34 mV) due to the presence of protonated amino groups of the dendrimer. The use of a higher generation amino-terminated dendrimer results in an increased zeta potential value (45 mV) due to a larger number of surface functional groups of dendrimer. The PbS nanocomposites using OH-terminated G4.0 dendrimer possess nearly equivalent positive charge (37 mV), whereas Si-$(OCH_3)_4$-terminated G4.0 dendrimer nanocomposites possess a slightly lower zeta potential value (24 mV). Furthermore, the instability of nanocomposites in the presence of excess sulfide concentration can be understood from the zeta potential values (Table 1). When the Pb^{2+}:S^{2-} ratio was 1:0.5 in the reaction mixture, PbS nanocomposites having larger zeta potential of 37 mV showed sufficient colloidal stability. The use of increasing sulfide ratio ($[Pb^{2+}]$:$[S^{2-}] \approx 1:2$) results in a decrease of the zeta potential value to 12 mV. When the zeta potential is low, attraction exceeds repulsion, and the dispersion will be hampered resulting in precipitation of aggregated PbS QDs.

The hybrid PbS nanocomposites are important for exciton migration owing to packing of PbS QDs and continuity offered by the dendrimer matrix.[33] Devices are constructed by using hybrid PbS/dendrimer nanocomposites to investigate the photoresponse characteristics. The device preparation was simple for this purpose, a thin film of nanocomposites has been fabricated by spin-casting on indium tin oxide (ITO) coated glass substrate (Aldrich, 70−100 Ω/squares inches). Sandwiched pattern devices have been fabricated by depositing aluminum by a vacuum deposition technique as the back electrode. A schematic illustration of the as-prepared device is shown in Figure 7a. In the present case, PbS nanocomposite-based devices were prepared without using any additional layers, which may enhance the photo response property.[34,35] Current−voltage (I−V) characteristics of the devices were recorded with a Keithley 2420 source meter in ambient conditions. The I−V characteristics in dark under 64.6 mW/cm^2 irradiation when exposed to an active area of 9 mm^2 are shown in Figure 7b. Upon illumination of light, the current increases exponentially, resulting in orders of an enhanced current compared to the dark measurement. In the dark, the current was only 0.025 mA at a bias voltage of 1 V. At an incident light density of 64.6 mW/cm^2 and a bias voltage of 1 V, the current jumps to 0.22 mA, giving a light/dark transformation ratio of ∼10. A control experiment with pure dendrimer does not show any photoresponse.

We have also studied the photo switching properties of this nanocomposites device without using any bias voltage at an incident light density of 25 mW/cm^2. Figure 7c shows the photocurrent switching from the device during repetitive on/off cycles of light illumination. The repetitive on−off device response to white illumination flux was found to be sharp, uniform, and repetitive over successive on/off cycles. The photocurrent increases and decreases as a response to the on/off operation and shows very high photosensitivity. After a number of cycles, the photocurrent can still be changed as a result of the illumination switching that shows its reproducibility. The long-term response characteristic of the constructed device is proven to be fairly stable and reversible. Further experiments show that the photocurrent is very sensitive and increases to the intensity of the incident light (Figure 7d).

A tiny change in light intensity can lead to a remarkable change in the photocurrent, which may lie in different photon densities from the incident lights. Figure 5d, shows that the device current in the absence of any bias voltage is strongly related to the light intensity and demonstrated a power dependence of ∼1.57 (i.e., $I \approx P^{1.57}$), indicating superior photocurrent capability of the PbS/dendrimer hybrid material. These results prove the promising potential of this device as a photoswitch and a highly photosensitive detector. It is worth noting that the applied bias voltage can also influence the on/off photoswitching performance of the devices, considering that the exciton dissociation and the background current usually

dx.doi.org/10.1021/jp210856n | J. Phys. Chem. C 2012, 116, 6022−6030

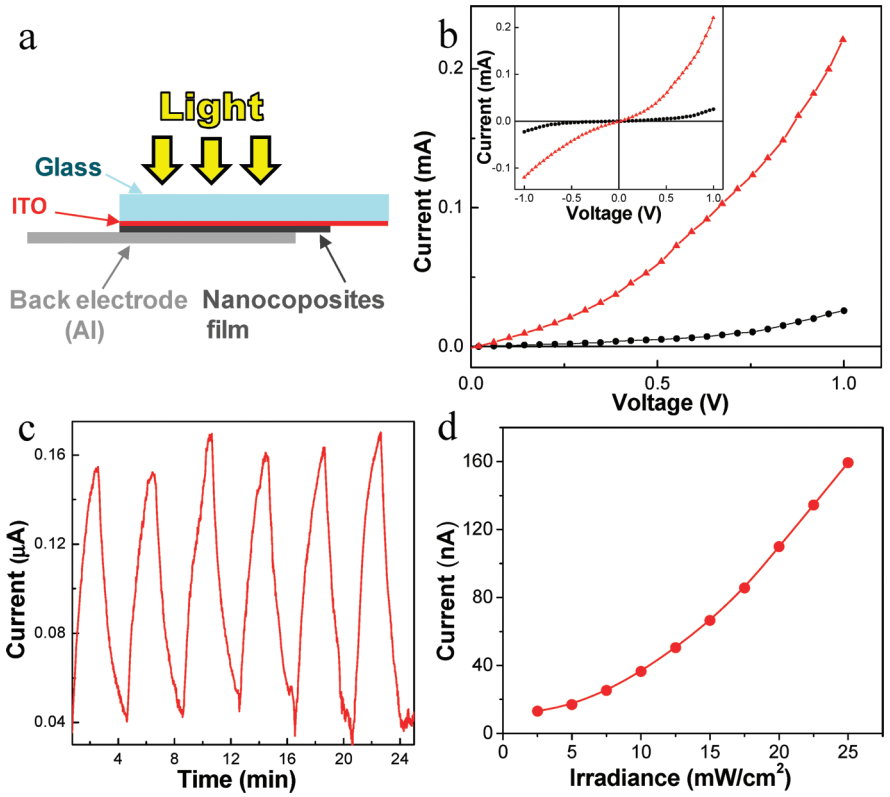

Figure 7. (a) Schematic illustration of the device fabrication using PbS/dendrimer nanocomposite. (b) Current−voltage characteristics of the nanocomposite device with irradiation (red up-triangle curve; incident light density, 64.6 mW/cm^2; bias voltage, 1 V) and in dark (black dotted curve) radiation. Inset: current−voltage characteristics in the bias voltage range −1 V to +1 V. (c) On/off switching of the nanocomposite device (incident light density, 25 mW/cm^2; bias voltage, 0 V). (d) Photocurrent versus incident light density in the absence of bias voltage.

depend on the applied bias voltage, then the switching performance will be faster.

4. CONCLUSIONS

In summary, we described a simple route of preparing PbS/dendrimer nanocomposites at ambient condition. PbS quantum dots of average diameter of 2.5−4.5 nm are designed in cubic crystallographic phase with a high degree of crystallinity. We showed that PbS QDs are bound to the surface functional groups of dendrimer molecules using FTIR spectroscopy. We showed the effect of dendrimer terminal groups on the formation of nanocomposites using functionalized hydroxyl-, amino-, and trimethoxysilyl-terminated dendrimers. The generation of dedrimer has a significant role in the dispersity of the PbS QDs within the nanocomposite. Thermal stability of the dendrimer molecule increases in the nanocomposite unit indicating strong interaction of inorganic phases with dendrimer. A combination of inorganic nanoparticles and dendritic polymer can be transformed into solid substrates as films for fabricating devices. A repetitive on/off device response to white illumination flux is found to be sharp and repeatable over successive on/off irradiation cycles, which is promising for large-area photodetector applications. The simple synthesis platform may provide an economic way to prepare unique PbS nanocomposites with potential applications as photodetectors.

■ ASSOCIATED CONTENT

Ⓢ Supporting Information

Energy dispersive X-ray spectrum, TEM image, and photoluminescence profiles. This material is available free of charge via the Internet at http://pubs.acs.org.

■ AUTHOR INFORMATION

Corresponding Author

*E-mail: camsa2@iacs.res.in.

Notes

The authors declare no competing financial interest.

■ ACKNOWLEDGMENTS

Financial support under Grant #SR/S5/NM-47/2005 and Grant# SR/NM/NS-49/2009 from DST, India, are gratefully acknowledged. S.G. is thankful to Dr A. Saha, UGC-DAE Consortium for Scientific Research, and Kolkata Centre for providing the dynamic light scattering and photoluminescence spectrophotometer facilities. A.H.K. is thankful to the Council of Scientific and Industrial Research, Government of India, for the award of Senior Research Fellowship.

■ REFERENCES

(1) (a) Tomczaka, N.; Janczewski, D.; Hana, M.; Vancsoa, G. J. *Prog. Polym. Sci.* **2009**, *34*, 393−430. (b) Li, J.; Zhang, J. Z. *Coord. Chem. Rev.* **2009**, *253*, 3015−3041. (c) Zhang, H.; Han, J.; Yang, B. *Adv. Funct. Mater.* **2010**, *20*, 1533−1550.

(2) Wang, T.; Keddie, J. L. *Adv. Colloid Interface Sci.* **2009**, *147−148*, 319−332.

(3) (a) Astruc, D.; Boisselier, E.; Ornelas, C. *Chem. Rev.* **2010**, *110*, 1857−1959. (b) Esfand, R.; Tomalia, D. A. *Drug Discovery Today* **2001**, *6*, 427−436. (c) Majoros, I.; Myc, A.; Thomas, T.; Mehta, C.; Baker, J. Jr. *Biomacromolecules* **2007**, *2*, 572−579. (d) Tekade, R. K.; Kumar, P. V.; Jain, N. K. *Chem. Rev.* **2009**, *109*, 49−87.
(4) (a) Vohsa, J. K.; Fahlman, B. D. *New J. Chem.* **2007**, *31*, 1041−1051. (b) Satoh, N.; Nakashima, T.; Kamikura, K.; Yamamoto, K. *Nat. Nanotechnol.* **2008**, *3*, 106−111. (c) Bronstein, L. M.; Shifrina, Z. B. *Chem. Rev.* **2011**, *111*, 5301−5344.
(5) (a) Jie, G.; Wang, L.; Yuan, J.; Zhang, S. *Anal. Chem.* **2011**, *83*, 3873−3880. (b) Juan, J. Y.; Jun, L. Y.; Ping, L. G.; Jie, L.; Feng, W. Y.; Qin, Y. R.; Ting, L. W. *Forensic Sci. Int.* **2008**, *179*, 34−38. (c) Crooks, R. M.; Chechik, V.; Lemon, B. I.; Sun, L.; Yeung, L. K.; Zhao, M. Synthesis, Characterization, and Applications of Dendrimer-Encapsulated Metal and Semiconductor Nanoparticles. In *Metal Nanoparticles: Synthesis, Characterization, and Applications*; Feldheim, D. L., Foss, C. A., Jr., Eds.; Dekker: New York, 2002; Chapter 6, pp 261−296. (d) Ghosh, S.; Bhattacharya, S. C.; Saha, A. *Anal. Bioanal. Chem.* **2010**, *397*, 1573−1582.
(6) Wu, X. C.; Bittner, A. M.; Kern, K. J. *J. Phys. Chem. B* **2005**, *109*, 230−239.
(7) (a) Lemon, B. I.; Crooks, R. M. *J. Am. Chem. Soc.* **2000**, *122*, 12886−12887. (b) Lakowicz, J. R.; Gryczynski, I.; Gryczynski, Z.; Murphy, C. J. *J. Phys. Chem. B* **1999**, *103*, 7613−7620. (c) Fahmi, A.; Pietsch, T.; Appelhans, D.; Gindy, N.; Voit, B. *New J. Chem.* **2009**, *33*, 703−706. (d) Ghosh, S.; Priyam, A.; Saha, A. *J. Nanosci. Nanotechnol.* **2009**, *9*, 6726−6735. (e) Zenga, Y.; et al. *Chem. Eng. J.* **2010**, *156*, 224−226.
(8) (a) Nakanishi, Y.; Ime, T. *J. Colloid Interface Sci.* **2005**, *285*, 158−162. (b) Qian, Z.; Bai, H.-J.; Wang, G.-L.; Xu, J.-J.; Chen, H.-Y. *Biosens. Bioelectron.* **2010**, *25*, 2045−2050. (c) Campos, B.; Algarra, M.; Esteves da Silva, J. C. G. *J. Fluoresc.* **2010**, *20*, 143−151. (d) Ghosh, S.; Ghosh, D.; Bag, P. K.; Bhattacharya, S. C.; Saha, A. *Nanoscale* **2011**, *3*, 1139−1148.
(9) Wang, D.; Imae, T. *Chem. Lett.* **2005**, *34*, 640−641.
(10) (a) Kanazawa, H.; Adachi, S. *J. Appl. Phys.* **1998**, *83*, 5997−6001. (b) Talapin, D. V.; Lee, J.-S.; Kovalenko, M. V.; Shevchenko, E. V. *Chem. Rev.* **2010**, *110*, 389−458.
(11) (a) Konstantatos, G.; Howard, I.; Fischer, A.; Hoogland, S.; Clifford, J.; Klem, E.; Levina, L.; Sargent, H. E. *Nature* **2006**, *442*, 180−183. (b) Peterson, J. J.; Krauss, T. D. *Nano Lett.* **2006**, *6*, 510−514. (c) Talapin, D. V.; Murray, C. B. *Science* **2005**, *310*, 86−89. (d) Mcdonald, S. A.; Konstantatos, G.; Zhang, S.; Cyr, P. W.; Klem, E. J. D.; Levina, L.; Sargent, E. H. *Nat. Mater.* **2005**, *9*, 1−5.
(12) (a) Kumar, A.; Jakhmola, A. *Langmuir* **2007**, *23*, 2916−2918. (b) Hinds, S.; Taft, B. J.; Levina, L.; Sukhovatkin, V.; Dooley, C. J.; Roy, M. D.; MacNeil, D. D.; Sargent, E. H.; Kelley, S. O. *J. Am. Chem. Soc.* **2006**, *128*, 64−65. (c) Bakshi, M. S.; Thakur, P.; Sachar, S.; Kaur, G.; Banipal, T. S.; Possmayer, F.; Petersen, N. O. *J. Phys. Chem. C* **2007**, *111*, 18087−18098.
(13) (a) Hines, M. A.; Scholes, G. D. *Adv. Mater.* **2003**, *15*, 1844−1849. (b) Abel, K. A.; Boyer, J. S. J. C.; Harris, F.; Van Veggel, F. C. J. M. *Chem. Mater.* **2008**, *20*, 3794−3796. (c) Moreels, I.; Lambert, K.; Smeets, D.; Muynck, D. D.; Nollet, T.; Martins, J. C.; Vanhaecke, F.; Vantomme, A.; Delerue, C.; Allan, G.; Hens, Z. *ACS Nano* **2009**, *3*, 3023−3033.
(14) (a) Zhao, X.; Gorelikov, I.; Musikhin, S.; Cauchi, S.; Sukhovatkin, V.; Sargent, E. H.; Kumacheva, E. *Langmuir* **2005**, *21*, 1086−1090. (b) Souici, A. H.; Keghouche, N.; Delaire, J. A.; Remita, H.; Etcheberry, A.; Mostafavi, M. *J. Phys. Chem. C* **2009**, *113*, 8050−8057.
(15) (a) Acharya, S.; Gautam, U. K.; Sasaki, T.; Bando, Y.; Golan, Y.; Ariga, K. *J. Am. Chem. Soc.* **2008**, *130*, 4594−4595. (b) Patla, I.; Acharya, S.; Zeiri, L.; Israelachvili, J.; Efrima, S.; Golan, Y. *Nano Lett.* **2007**, *7*, 1459−1462. (c) Acharya, S.; Sarma, D. D.; Golan, Y.; Sengupta, S.; Ariga, K. *J. Am. Chem. Soc.* **2009**, *131*, 11282−11283.
(16) (a) Vossmeyer, T.; Jia, S.; Delono, E.; Diehl, M. R.; Kim, S. H.; Peng, X.; Alivisatos, A. P.; Heath, J. R. *J. Appl. Phys.* **1998**, *84*, 3664−3670. (b) Rogach, A. L.; Susha, A. S.; Caruso, F.; Sukhorukov, G. B.; Kornowski, A.; Kershaw, S.; Möhwald, H.; Eychmüller, A.; Weller, H. *Adv. Mater.* **2000**, *12*, 333−337.
(17) Lu, C.; Wu, N.; Wei, F.; Zhao, X.; Jiao, X.; Xu, J.; Luo, C.; Cao, W. *Adv. Funct. Mater.* **2003**, *13*, 548−552.
(18) (a) Wu, X. C.; Bittner, A. M.; Kern, K. *Adv. Mater.* **2004**, *16*, 413−417. (b) Wang, Y.; Xie, X.; Goodson, T. III. *Nano Lett.* **2005**, *5*, 2379−2384. (c) Shi, X.; Wang, S. H.; Lee, I.; Shen, M.; Baker, J. R. Jr. *Biopolymers* **2009**, *11*, 936−942. (d) Shi, X.; Wang, S.; Meshinchi, S.; Antwerp, M. V.; Bi, X.; Lee, I.; Baker, J. R. Jr. *Small* **2007**, *3*, 1245−1252.
(19) (a) Lo, S.-C.; Burn, P. L *Chem. Rev.* **2007**, *107*, 1097−1116. (b) Tomalia, D. A.; Nayor, A.; Goddard, W. I. *Angew. Chem., Int. Ed.* **1990**, *29*, 138−175. (c) Gillies, E. R.; Fréchet, J. M. J. *Drug Discovery Today* **2005**, *10*, 35−43.
(20) Tan, W.; Zhou, J.; Li, F.; Yi, T.; Tian, H. *Chem. Asian J.* **2011**, *6*, 1263−1268.
(21) Priyam, A.; Ghosh, S.; Bhattacharya, S. C.; Saha, A. *J. Colloid Interface Sci.* **2009**, *331*, 195−201.
(22) Talapin, D. V.; Rogach, A. L.; Haase, M.; Weller, H. *J. Phys. Chem. B* **2001**, *105*, 12278−12285.
(23) Peng, X.; Wickham, J.; Alivisatos, A. P. *J. Am. Chem. Soc.* **1998**, *120*, 5343−5344.
(24) Ghosh, S.; Datta, A.; Saha, A. *Colloids Surf., A* **2009**, *355*, 130−138.
(25) (a) Ishida, K. P.; Griffiths, P. R. *Appl. Spectrosc.* **1993**, *47*, 584−589. (b) Weert, M. V.; Haris, P. I.; Hennink, W. E.; Crommelin, D. J. A. *Anal. Biochem.* **2001**, *297*, 160−169. (c) Pevsner, A.; Diem, M. *Appl. Spectrosc.* **2001**, *55*, 788−793. (d) Rahmelow, K.; Hübner, W. A. *Appl. Spectrosc.* **1997**, *51*, 160−170.
(26) Sooklal, K.; Hanus, L. H.; Pleohn, H. J.; Murphy, C. J. *Adv. Mater.* **1998**, *10*, 1083−1087.
(27) (a) Ozturk, O.; Black, T. J.; Perrine, K.; Pizzolato, K.; Williams, C. T.; Parsons, F. W.; Ratliff, J. S.; Gao, J.; Murphy, C. J.; Xie, H.; Ploehn, H. J.; Chen, D. A. *Langmuir* **2005**, *21*, 3998−4006. (b) Lang, H.; May, R. A.; Iversen, B. L.; Chandler, B. D. *J. Am. Chem. Soc.* **2003**, *125*, 14832−14836. (c) Deutsch, D. S.; Lafaye, G.; Liu, D.; Chandler, B.; Williams, C. T.; Amiridis, M. D. *Catal. Lett.* **2004**, *97*, 139−142.
(28) Khan, A. H.; Ji, Q.; Ariga, K.; Thupakula, U.; Acharya, S. *J. Mater. Chem.* **2011**, *21*, 5671−5676.
(29) Nair, S.; Radhakrishnan, T.; Revaprasadu, N.; Kolawole, G. A.; Luyt, A. S.; Djokoví, V. *Appl. Phys. A: Mater. Sci. Process.* **2005**, *81*, 835−837.
(30) Dvornic, P. R.; de Leuze-Jallouli, A.; Owen, M. J.; Perz, S. V. *Macromolecules* **2000**, *33*, 5366−5378.
(31) Dvornic, P. R.; de Leuze-Jallouli; A.; Owen, M. J.; Perz, S. V. Dendrimer-Based Networks Containing Lyophilic Organosilicon and Hydrophilic Poly(amidoamine) Nanoscopic Domains. U.S. Patent 5,902,863, 1999.
(32) (a) Ghosh, S.; Priyam, A.; Saha, A. *J. Nanosci. Nanotechnol.* **2009**, *9*, 6726−6735. (b) Ilhelm, C.; Billotey, C.; Roger, J.; Pons, J. N.; Bacri, J. C.; Gazeau, F. *Biomaterials* **2003**, *24*, 1001−1011.
(33) Pijpers, J. J. H.; Ulbricht, R.; Tielrooij, K. J.; Osherov, A.; Golan, Y.; Delerue, C.; Allan, G.; Bonn, M. *Nat. Phys.* **2009**, *5*, 811−814.
(34) Sukhovatkin, V.; Hinds, S.; Brzozowski, L.; Sargent, E. H. *Science* **2009**, *324*, 1542−1544.
(35) Tang, J.; Sargent, E. H. *Adv. Mater.* **2011**, *23*, 12−29.